STAR Note 243

Two-Photon Physics with STAR

Spencer Klein and Evan Scannapieco
Lawrence Berkeley National Laboratory
March 22, 1996
Version 1.01: May 13, 1996

Abstract

We present a study of two-photon interactions at STAR. The effective $\gamma\gamma$ luminosity is calculated and rates are presented for many final states. A two-photon Monte Carlo is described, and estimates of STAR acceptance calculated. The expected backgrounds due to peripheral nuclear collisions and beam-gas are given, along with three sample analyses. Finally, a scheme for STAR to trigger on these events is presented.

1 Introduction

While most of the STAR collaboration has focused on central collisions, we wish to point out that there is interesting physics present in peripheral collisions, and STAR is well suited to studying much of this physics.

Peripheral collisions cover a wide range of topics. Two-photon interactions probe the charge content of a wide range of final states: charmed and uncharmed mesons, meson, baryon and lepton pairs, jets; anything containing charge. Studies of charmed quark production in photon-gluon collisions may provide an alternative method to measure the gluon structure function in heavy nuclei[12][16]. Photon-gluon interactions deep inside nuclei may also provide a way to study nuclear medium effects on meson masses and branching ratios. And, coherent interactions involving Pomerons offer us the opportunity to study Pomerons, and their coherent coupling to nuclei[9] [22].

Much of this physics is unique to RHIC. Because RHIC will be the first nuclear accelerator with the energy to study these processes, the experimental framework for these studies is needs to be developed. This memo will discuss the physics interest and feasibility of the best understood topic: two-photon physics. After general introductions to the physics processes and backgrounds, we will give several concrete examples of physics that might be studied by STAR.

Two-photon interactions occur when the virtual photon fields carried by the two nuclei collide. Because photons couple to charge, almost any charge containing final state can be produced. This physics is especially attractive at RHIC because the fields from the protons in a single nucleus add coherently, so the fields scale as Z^2, and the interaction rate as Z^4. Therefore, despite the relatively low nuclear luminosity, RHIC produces a very large $\gamma\gamma$ interaction rate.

The main disadvantage to heavy ion colliders is that, when the photon energies are larger than the size of the nucleus, $\gamma\hbar/R$ (in the lab frame), then the electromagnetic field of the nucleons lose coherence, and the luminosity drops. At RHIC, this occurs at $\gamma\gamma$ center of mass energies, W above about 6 GeV. Another disadvantage is that, in collisions where the nuclei interact hadronically as well as electromagnetically the hadronic interaction will obscure the electromagnetic interactions. Because these collisions are unusable for studying $\gamma\gamma$ processes, they are omitted from the event rate calculations that follow.

In the past, $\gamma\gamma$ physics has been studied extensively at e^+e^- colliders[7][19]. Because of the Z^4 enhancement, RHIC will be able produce a larger $\gamma\gamma$ luminosity than existing and planned e^+e^- colliders up to $\gamma\gamma$ energies of a few GeV.

Because RHIC will be the first heavy ion accelerator with enough energy to study $\gamma\gamma$ reactions that produce hadronic final states, there has been considerable uncertainty as to whether the interesting measurements are indeed feasible. This memo will attempt to answer this question, with particular emphasis on the STAR detector.

After reviewing some of the interesting physics, we describe the $\gamma\gamma$ luminosity calculations. We calculate the $\gamma\gamma$ luminosity curves for various nuclear beams, and event rates for some interesting final states. We then discuss a $\gamma\gamma$ Monte Carlo, STARlight that we have written, and calculate the efficiency for STAR to detect these final states. We then discuss various background sources, and estimate the rates from these sources, presenting a number of sample calculations of expected signal to noise ratios. Finally, we propose algorithms for STAR to trigger on these events.

2 Physics Interest

Two-photon physics covers a broad range of topics. Because photons couple to charge, two photons can combine to produce almost any spin 0 or 2 (if one of the photons is far off mass shell, spin 1 final states are also possible) charge containing final state. Some of the channels accessible to STAR include: single charmed and uncharmed mesons, meson and baryon pairs, and lepton pairs.

Because the STAR TPC is at a more advanced stage than the calorimeter, this note will focus on interactions that produce all charged particle final states, using the calorimeter only as a veto. There is an equally interesting set of final states involving photons. As the calorimeter evolves and manpower becomes available, we will consider these reactions. Similarly, non-resonant pair production is best studied with forward detectors; because the FTPC design is at an early stage, these interactions will be given relatively little attention here.

2.1 Single Mesons

One of the most interesting physics topics is the study of single meson production for mesons in the 1 to 2 GeV mass range. QCD makes clear predictions about the number of mesons, and gives estimates of their masses. However, in the 1 to 2 GeV range, there are many more observed particles than can fit into the expected spectrum. The obvious explanations include the possibility of bad data, a problem in the standard model, or that some sort of exotic particles are being produced, such as four quark states, mixed states ($q\overline{q}g$ hybrids) or glueballs. Two-photon interactions provide a good probe of the charge content of states; a glueball would be expected to have a small coupling to two photons.

The particle data group recently reviewed the experimental situation in the 1-2 GeV region[21]. For $J^{PC} = 0^{++}$, the quark model predicts two 1^3P0 and one 2^3P0 states below 1.8 GeV. However, 5 candidates are observed: the $f_0(980)$, $f_0(1300)$, $f_0(1370)$, $f_0(1590)$ and the $f_J(1710)$. The $f_0(1590)$, seen in πp reactions, has peculiar decay ratios. The $f_J(1710)$ has been seen in J/ψ decays, but not in $\gamma\gamma$ fusion. For these reasons, the latter two states are candidates to be some sort of exotic particle. Better limits on their coupling to $\gamma\gamma$ would provide evidence that the states have a large gluon content. Because of the high RHIC $\gamma\gamma$ luminosity, STAR can push these limits downward, or measure the coupling.

The situation is similar for $J^{PC} = 2^{-+}$ states; more mesons than fit into the standard model; the $f_2(1430)$, $f_2(1520)$, and $f_2(1810)$ are candidates as exotica.

Typical production rates for normal $q\overline{q}$ mesons is 100,000-1,000,000 mesons/year at RHIC; depending on masses, branching ratios and widths, STAR could detect signals down to a few percent of the standard coupling.

2.2 Meson pairs

Large numbers of meson pairs are produced by the reaction $\gamma\gamma \rightarrow h^+h^-$. Because the production is diffractive, most of the particles go down the beampipe. However, the rates are high enough that useful numbers can be detected centrally. The major physics interest is in studying the hadron to quark transition. Near threshold, the final states are best described in terms of hadrons. Since photons couple to charge, $\pi^+\pi^-$ are produced, but not $\pi^0\pi^0$. At high energies, where a quark description is appropriate, similar numbers of $\pi^+\pi^-$ and $\pi^0\pi^0$ are produced. By studying the rates as a function of pair mass, the transition region can be probed. While this has been done for the more copiously produced mesons, STAR could study K^0s, K*s and other mesons.

$\rho^0\rho^0$ pairs near threshold are of special interest. Many e^+e^- experiments have observed a resonance-like structure in $\gamma\gamma \rightarrow 4\pi$, dominated by $\rho^0\rho^0$. To quote a mini-review in the 1994 particle data book[21], "This process has not been explained by models in which only conventional resonances dominate". Taking advantage of its greatly increased luminosity, STAR could map out the resonance shape in detail, and look for decays to other channels.

2.3 Baryon pairs

In the early days of fragmentation studies at e^+e^- colliders, the high rate of baryon production was a big surprise; typically 10% of the particles were baryons. To explain this, modelers postulated that, in addition to quark-antiquark pairs, diquark-anti-diquark pairs could be produced when color strings break. There has been much debate over the 'reality' of diquarks and this model, but it does seem to fit the data well. Measurements of $\gamma\gamma \rightarrow p\overline{p}$ at e^+e^- colliders match the diquark predictions; STAR could contribute by measuring Λ, Ξ, Σ^* and other baryon pairs.

2.4 Lepton pairs

Lepton pairs can be useful as a calibration. Electron and muon pairs provide a method for checking the $\gamma\gamma$ luminosity calculations. Electron production at low momentum is an extremely interesting physics topic, because $Z\alpha$ is large, and so electron production is a test of strong field QED. Unfortunately, it does not appear that STAR can reach low enough momenta to study this physics. τ pairs are also produced, but the rates are not large.

Once lepton pairs have been well studied, they may be useful as a relative luminosity monitor. The rates are high enough (> 1 Hz) that good statistics can be accumulated with relatively short runs.

2.5 Other physics

X.N. Wang has suggested that it may be possible to detect the σ field, expected to have a mass of a few hundred MeV, by its coupling to two photons, and decay to $\pi^0\pi^0$[26]. There is also extensive literature on the possibility of production of lepton pairs followed by capture. However, one line of argument suggests that this is only possible for electrons[17]. Many other physics topics are clearly possible.

Many of the analysis techniques, background calculations and triggering schemes presented here are relevant to studies of coherent Pomeron interactions. Because of the coherent couplings, the two interactions display similar kinematics and are therefore difficult to distinguish experimentally. The only significant external difference is that photons, since they couple to charge, and hence to protons only, are likely to leave the nucleus excited in a giant dipole resonance, while Pomerons, coupling to both protons and neutrons, are much less likely to do so. Although it is outside the scope of this note, the interplay and possible interference between the two interactions is of strong interest. More theoretical work is needed here, but, as experimentalists, we should make the measurements and let the theorists sort out the detailed theory.

This note presents a preliminary study of $\gamma\gamma$ interactions at STAR. We begin with a discussion of the physics of $\gamma\gamma$ interactions and the calculation of production cross sections for various final states. Section 3 presents $\gamma\gamma$ luminosity curves and rapidity distributions and cross-sections and event rates for the $\gamma\gamma$ production of mesons and muon and tau pairs. Section 4 describes the $\gamma\gamma$ Monte Carlo program which is used to calculate acceptances given in Section 5. Section 6 discusses the backgrounds to $\gamma\gamma$ collisions and their modeling with FRITIOF and VENUS. These codes are used to conduct sample analyses in section 7 and to examine trigger rates in section 8. Section 9 summarizes our conclusions.

3 Luminosity Calculation

The virtual (but nearly real) γ flux accompanying a heavy nucleus is given by the Weizsäcker Williams approximation [15]. Classically, the equivalent photon spectrum as a function of impact parameter b is[15]

$$\frac{d^2f}{db^2}(b,E) = \frac{Z^2\alpha}{\pi^2}\left(\frac{E}{\gamma}\right)^2\frac{1}{\beta^4}\left(K_1^2(x)+\frac{1}{\gamma^2}K_0^2(x)\right) \tag{1}$$

where Z is the nuclear charge, α the fine structure constant, E the photon energy, β the nuclear velocity, and $\gamma = \sqrt{1-\beta^2}$. $x \equiv \frac{Eb}{\gamma\beta}$, and K_0 and K_1 are modified Bessel functions of order zero and one. The Bessel functions provide the previously described cutoff for photon energies $> \hbar R/\gamma$. Here and below, we omit all factors of $\hbar$ and c. The Weizsäcker Williams approximation treats the virtual photons as massless; for nuclear fields at RHIC energies, this is a good approximation.

By taking $\beta \approx 1$, neglecting the $1/\gamma^2$ term, and integrating this equation over impact parameters from R to infinity, the photon distribution can be computed exactly. The integration is begun at R to exclude interactions which occur inside the nucleus.

$$f_{cl}(E) = \frac{2Z^2\alpha}{\pi}\left(XK_0(X)K_1(X) - \frac{X^2}{2}\left(K_1^2(X) - K_0^2(X)\right)\right) \tag{2}$$

where $X \equiv \frac{ER}{\gamma}$ and R is the nuclear radius.

To calculate an overall $\gamma\gamma$ luminosity, it is necessary to integrate over all space and over all impact parameters. This introduces one important complication. When the nuclei physically collide ($b < 2R$), then the hadronic interactions will completely overshadow the electromagnetic ones. Therefore, in calculating the usable $\gamma\gamma$ luminosity, this overlap region must be excluded. Cahn and Jackson proposed a method to do this[8]. They define a dimensionless $\gamma\gamma$ luminosity F such that

$$L_{\gamma\gamma}(W,Y) = L_{NN}F(W,Y) \tag{3}$$

where $L_{\gamma\gamma}$ is the $\gamma\gamma$ luminosity and L_{NN} the nucleus-nucleus luminosity. $F(W,Y)$ is given by the products of the equivalent photon spectrum of the two ions, excluding the overlap region; Cahn and Jackson calculated this by finding the complete overlap, which separates into the product of the $\gamma\gamma$ spectra, and subtracting a correction term for the region of nuclear overlap $b < 2R$:

$$F(E_1,E_2) = f_{cl}(E_1)f_{cl}(E_2) - \Delta F(E_1,E_2) \tag{4}$$

where E_1 and E_2 are the photon energies, f_{cl} is the classical photon distribution given above, and ΔF is the overlap correction, excluding interactions within the nuclei.

ΔF, the correction term for the interacting fields, must be computed by numerically integrating the overlap expression:

$$\Delta F(E_1,E_2) = 4\pi\int_R^\infty b_1 db_1 \int_{b_{min}}^{b_1+2R} b_2 db_2 \frac{d^2 f}{db_1^2}(b_1,E_1)\frac{d^2 f}{db_2^2}(b_2,E_2)\arccos\left(\frac{b_1^2+b_2^2-4R^2}{2b_1b_2}\right) \tag{5}$$

where b_{min} is the larger of $b_1 - 2R$ and R. A similar approach was followed by Baur and Ferreira Filho[2].

This analysis excludes particle production inside the nucleus. This avoids uncertainties due to the nuclear form factor and possible particle absorption in the nucleus. Including interactions in the nucleus would lead to a small increase in effective luminosity.

With appropriate substitutions, the frequency distribution can be re-expressed as a differential luminosity as function of rapidity $Y = 1/2\ln(E_1/E_2)$ and center of mass energy of the $\gamma\gamma$ system $W = 4E_1E_2$:

$$\frac{d^2F}{dWdY}(W,Y) = \frac{2}{W}F\left(\frac{W}{2}\exp(Y), \frac{W}{2}\exp(-Y)\right). \tag{6}$$

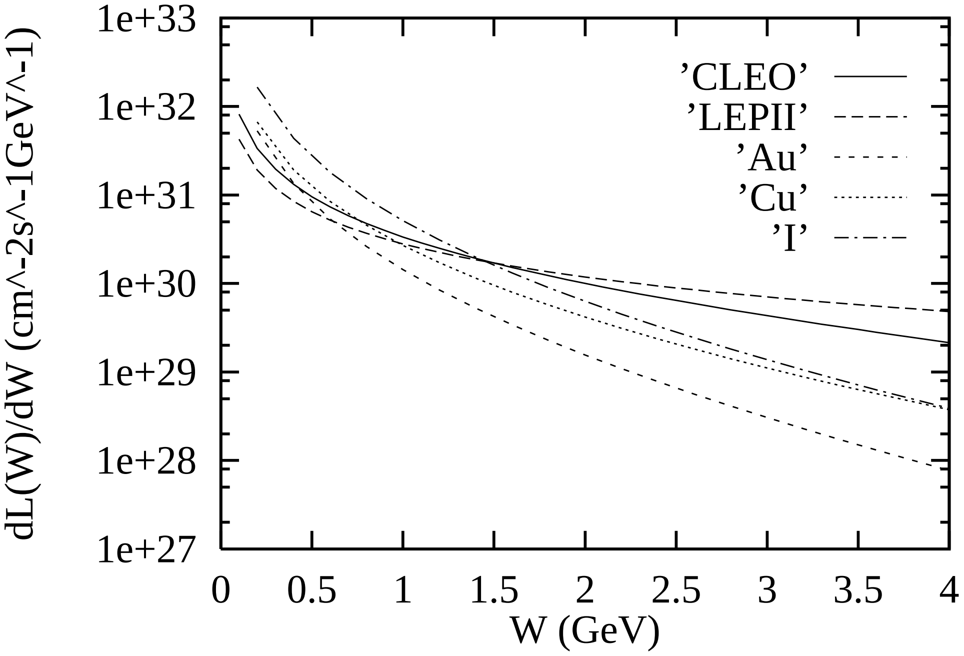

Figure 1: Comparison of $\gamma\gamma$ luminosities at RHIC with those of CESR(CLEO) and LEP II, for gold, iodine and copper beams.

This function was calculated using a program that was written by Kai Hencken[14], originally for use at the LHC; the numerical evaluation uses Gaussian integration.

The luminosities for RHIC are shown in Figure 1 as a function of center of mass energy W. Nuclear radii are taken to be $1.2 \times A^{1/3}$ fm. The three curves are for gold ($\gamma = 100$, luminosity = 2.0 $\times 10^{26}$ cm^{-2} s^{-1}), iodine ($\gamma = 104$, luminosity = 2.7 $\times 10^{27}$ cm^{-2} s^{-1}) and copper ($\gamma = 115$, luminosity = 9.5 $\times 10^{27}$ cm^{-2} s^{-1}), where the γs and luminosities come from the RHIC Conceptual Design Report[10]. The $\gamma\gamma$ luminosities are higher for iodine and copper than gold because of the higher nuclear luminosities and the smaller nuclear sizes. Also shown are the expectations for the CESR (CLEO experiment) e^+e^- and LEP II colliders, calculated using[14]

$$\frac{dL(W,s)}{dW} = \left(\frac{\alpha}{2\pi}\ln\left(\frac{s}{4m_e^2}\right)\right)^2 \frac{2}{W}\left((2+\tau)^2\ln\left(\frac{1}{\tau}\right) - 2(1-\tau)(3+\tau)\right) \tag{7}$$

where $\tau = W^2/s$ and $\sqrt{s}$ is the center of mass energy of the e^+e^- system. Here $s = 100$ GeV^2 and the e^+e^- luminosity is 2.9 $\times 10^{32}$ cm^{-2} s^{-1} [21] for CESR and s=$(180GeV)^2$ and the e^+e^- luminosity is 5×10^{31} for LEP II[11]. RHIC outshines the e^+e^- colliders up to about 1 GeV.

For the e^+e^- colliders, the final states are spread over a wider rapidity range than at RHIC, because of the absence of a photon energy cutoff. Requiring that the final state be produced at a rapidity less than 1, not unreasonable for a multiple particle system for example, reduces the $\gamma\gamma$ luminosity at CESR and LEP II by about 40%, for example.

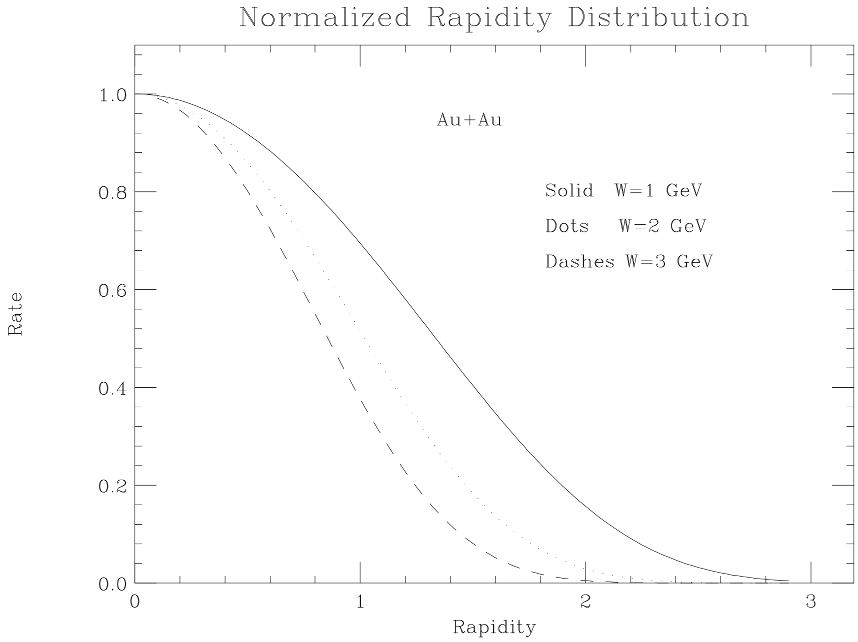

Figure 2: Rapidity distribution of produced particles for gold on gold collisions with $W = 1$, 2 and 3 GeV.

Figures 2 and 3 show the differential luminosity as a function of rapidity for fixed center of mass energies of 1, 2, and 3 GeV for gold and copper respectively.

These luminosities are much lower, and the Y distributions are much narrower than those in Baron and Baur[1]. This discrepancy may be due to a dropped $\hbar c$ by Baron and Baur in the calculation of $X \equiv \frac{ER}{\gamma \hbar c}$. The same error was made in the Klein 1995 paper[17].

4 Production Rates at RHIC

The program was used to calculate the production rates for various mesons as well as $\mu^+\mu^-$, $\tau^+\tau^-$, and $\rho^0\rho^0$ pairs near threshold. Single meson production cross sections were calculated with W fixed at the meson mass, and numerically integrating over rapidity, with the rate dependent on the spin and two-photon partial width $\Gamma_{\gamma\gamma}$[3]

$$\sigma = \int_{-\infty}^{\infty} dY \, 8\pi(2J+1)\Gamma_{\gamma\gamma} \left(\frac{1}{M}\right)^2 \frac{d^2F}{dWdY}(M,Y) \tag{8}$$

where M and J are the mass and spin of the meson.

The total lepton pair rates were computed by integrating over both Y and W, from the energy threshold to infinity, using the formula given in Soff *et al.*[24]:

$$\sigma_{\ell^+\ell^-}(W) = 4\pi\alpha^2 \frac{1}{s} \left(\left(1 + \frac{4m^2}{s} - \frac{8m^4}{s^2}\right) L - \left(\frac{1}{s} + \frac{4m^2}{s^2}\right) \Delta t \right) \tag{9}$$

where

$$\Delta t = s\sqrt{1 - \frac{4m^2}{s}} \ , \ \ L = 2\ln\left(\frac{\sqrt{s}}{2m} + \sqrt{\frac{s}{4m^2} - 1}\right) \ ,$$

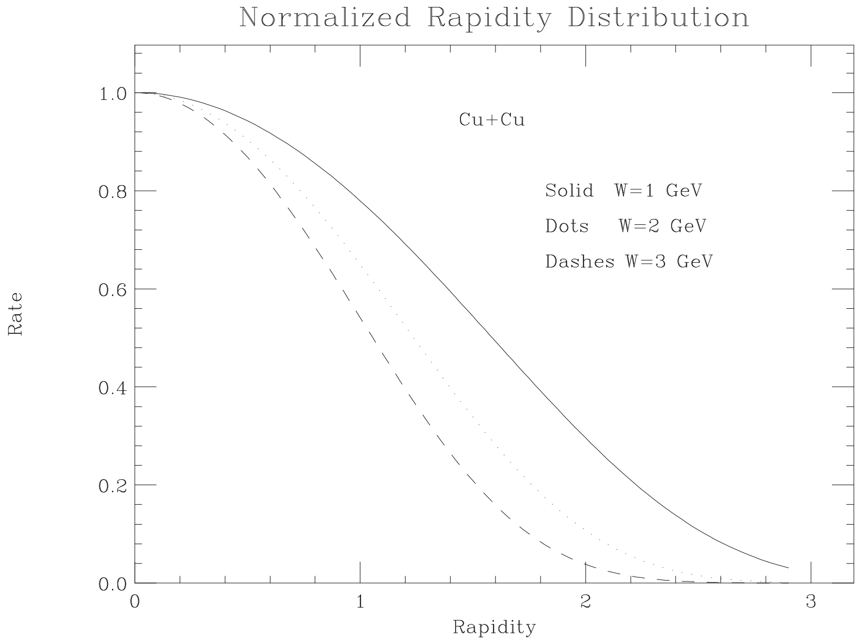

Figure 3: Rapidity distribution of produced particles for copper on copper collisions with W = 1, 2 and 3 GeV. These distributions are wider than in Figure 2 because copper is smaller, and hence has a higher energy photon cutoff.

$s = W^2$, and m is the lepton mass. Thus the total lepton pair cross sections are

$$\sigma = \int_{4m^2}^{\infty} dW \int_{-\infty}^{\infty} dY \sigma_{\ell^+\ell^-}(W) \frac{d^2F}{dWdY}(W,Y). \tag{10}$$

The production of $\rho\rho$ pairs near threshold (1.5-1.6 GeV) was based on the rates measured by Berger *et al.*[4]. They measured $\sigma_{\gamma\gamma\rightarrow\pi^+\pi^-\pi^+\pi^-}(E) = 133\pm14$ nb in the 1.5-1.6 GeV energy range, with $72 \pm 14\%$ of this coming from ρ pairs. The total production cross section of ρ pairs near threshold was taken to be

$$\sigma = \int_{1.5GeV}^{1.6GeV} dW \int_{-\infty}^{\infty} dY \sigma_{\rho\rho^0} \frac{d^2F}{dWdY}(W,Y). \tag{11}$$

with $\sigma_{\rho^0\rho^0} = 100$ nb.

Table 1 gives $\gamma\gamma$ production cross sections at RHIC for muon, tau, and rho pairs and a number of mesons. To give some indication of the dependence on the ions used, cross sections are calculated for gold, iodine and copper beams. The $\gamma\gamma$ widths ($\Gamma_{\gamma\gamma}$) are from the 1994 particle data book. These cross sections were used to calculate the expected event rates given in Table 2 for different heavy ions, assuming 10^7 seconds of operation per year.

5 Monte Carlo Simulation

To go much farther than simple rate calculations requires a Monte Carlo. We have developed a Monte Carlo with a production mechanism based on the preceding luminosity calculations.

Name	Spin	Mass (GeV)	$\Gamma_{\gamma\gamma}$ (keV)	$\sigma_{AuAu}(b)$ ($\gamma = 100$)	$\sigma_{II}(b)$ ($\gamma = 104$)	$\sigma_{CuCu}(b)$ ($\gamma = 115$)	$\sigma_{SiSi}(b)$ ($\gamma = 125$)
η_c	0	2.981	6.3	3.7×10^{-6}	1.2×10^{-6}	2.8×10^{-7}	3.3×10^{-8}
η'	0	0.958	4.3	1.4×10^{-3}	3.8×10^{-4}	5.7×10^{-5}	4.4×10^{-6}
f_0	0	0.975	0.56	1.5×10^{-4}	3.9×10^{-5}	5.9×10^{-6}	5.1×10^{-7}
f_2	2	1.270	2.6	9.3×10^{-4}	2.6×10^{-4}	4.2×10^{-5}	3.8×10^{-6}
a_2	2	1.320	1.0	3.1×10^{-4}	8.5×10^{-5}	1.4×10^{-5}	1.3×10^{-6}
f_2	2	1.525	0.1	1.4×10^{-5}	4.0×10^{-6}	6.8×10^{-7}	6.5×10^{-8}
$\mu^+\mu^-$	—	>0.21 MeV	—	3.0×10^{-1}	7.5×10^{-2}	9.5×10^{-3}	7.2×10^{-4}
$\tau^+\tau^-$	—	>3.56	—	9.4×10^{-7}	3.5×10^{-7}	1.0×10^{-7}	1.4×10^{-8}
$\rho^0\rho^0$	—	1.5-1.6	—	2.1×10^{-5}	5.9×10^{-6}	1.0×10^{-6}	1.0×10^{-7}

Table 1: Two-photon production cross sections (in barns) for muon and tau pairs and various mesons at RHIC. ρ^0 pair cross sections given only near threshold (1.5-1.6 GeV range).

		Thousands of Events / Year								Evt / s
Ion	Luminosity (cm^{-2} s^{-1})	η_c	η'	f_0 975	f_2 1270	a_2 1320	f_2 1525	$\rho^0\rho^0$	$\tau^+\tau^-$	$\mu^+\mu^-$
Au	2.0×10^{26}	7.4	2,800	300	1,900	620	28	42	1.9	60
I	2.7×10^{27}	32	10,000	1,000	7,000	2,300	110	160	9.5	200
Cu	9.5×10^{27}	27	5,400	510	4,000	1,300	65	90	9.5	90
Si	4.4×10^{28}	15	1,900	220	1,700	570	29	44	6.2	32

Table 2: Production rates for particles produced in $\gamma\gamma$ collisions at RHIC.

The program begins by generating normalized arrays of integral cross sections (not shown here) as a function of W and Y of the $\gamma\gamma$ system. For meson and ρ pair production, the array is one dimensional:

$$\frac{\int_0^Y dY' \frac{d^2F}{dWdY'}(M,Y')}{\int_0^\infty dY' \frac{d^2F}{dWdY'}(M,Y')}$$

A random number is generated, and compared with the above array to find the $|Y|$ of the event. Linear interpolation is used between the two nearest entries. Finally, the sign of Y is chosen randomly.

The production of $\mu^+\mu^-$ and $\tau^+\tau^-$ pairs is more complicated as both the center of mass energy and rapidity must be found. Here, a two step process is used. First W is determined by comparing a random number to a table of

$$\frac{\int_{4m^2}^W \int_0^\infty dYdW'\sigma_{\ell^+\ell^-}(W')\frac{d^2F}{dWdY}(W',Y)}{\int_{4m^2}^\infty \int_0^\infty dYdW'\sigma_{\ell^+\ell^-}(W')\frac{d^2F}{dWdY}(W',Y)}$$

where $\sigma_{\ell^+\ell^-}(W)$ is as given in Equation 9. Then this value, W_0, is used to determine Y by comparing another random number to a table of values of

$$\frac{\int_0^Y dY' \frac{d^2F}{dWdY}(W_0,Y')}{\int_0^\infty dY' \frac{d^2F}{dWdY}(W_0,Y')}$$

and randomly assigning the sign of Y.

Using these values of Y and W, the momenta of the incoming photons are calculated as

$$E_1 = \frac{We^Y}{2}, \quad E_2 = \frac{-We^{-Y}}{2}.$$

The momentum along the beamline of the $\gamma\gamma$ system is

$$E_1 + E_2 = W \sinh Y. \tag{12}$$

The transverse momenta of the photons is zero in the classical approach of the equivalent photon spectra Eq. 1. Transverse momentum spectra are included using the approach suggested in Hencken [14]. The distribution of photons as a function of E and $p_\perp$ is

$$\frac{dN(E,p_\perp)}{dp_\perp} = \frac{2F^2p_\perp^3}{(2\pi)^2\left((E/\gamma)^2+p_\perp^2\right)^2} \tag{13}$$

Hencken found $N(E)$ by using a point charge form factor and integrating $\frac{dN(E,p_\perp)}{dp_\perp}$ from $p\perp = 0$ to $p\perp = 1/R$. The 1/R cutoff comes from the same coherence requirement that limits the longitudinal momentum to γR. Unfortunately, the hard $1/R$ cutoff is somewhat unphysical, as can be seen in Figures 4 and 5.

A better approach is to use a Gaussian form factor with a characteristic width of 1/R. In this case $F = e^{-(p_\perp R)^2}$ resulting in the dotted curves in Figures 4 and 5. In the Monte Carlo a cut-off is placed at 1.5/R GeV, which is high enough to avoid an sharp unphysical drop

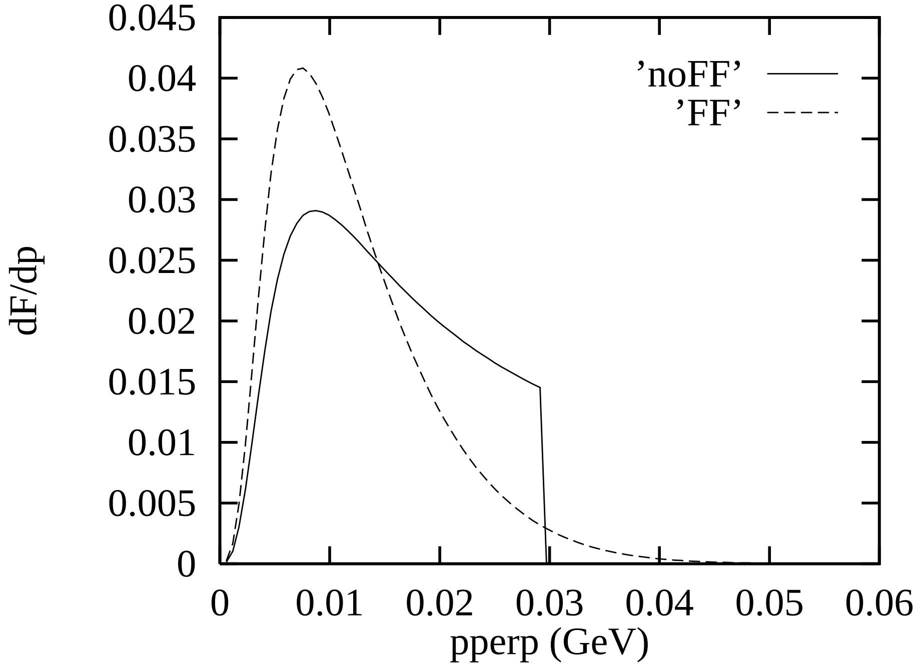

Figure 4: Comparison of point charge versus Gaussian form factor $p_\perp$ distributions for gold ($R = 6.8$ fm), $\gamma = 100$, $E = 0.5$ GeV.

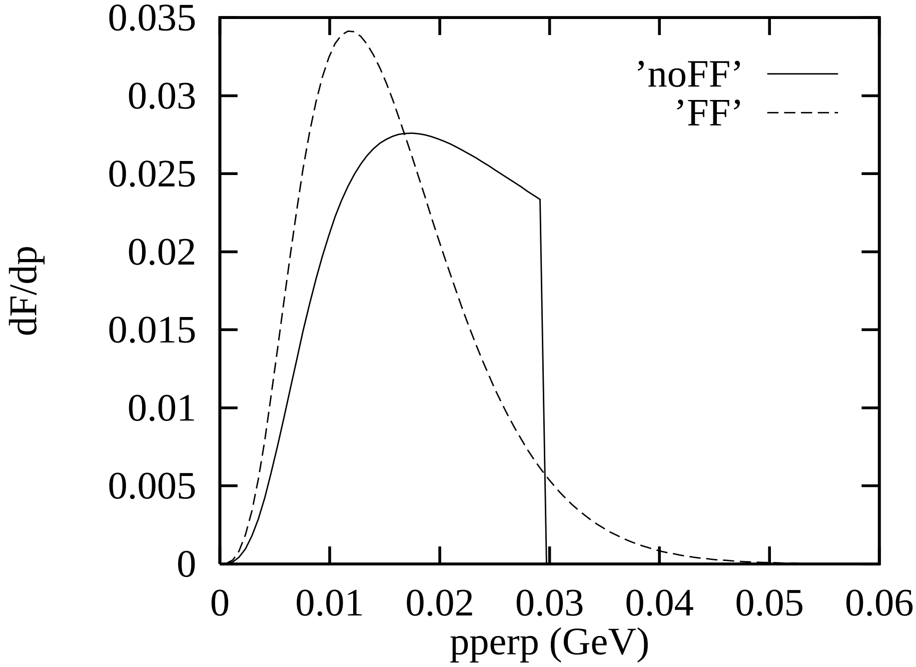

Figure 5: Comparison of point charge versus Gaussian form factor $p_\perp$ distributions for gold ($R = 6.8$ fm), $\gamma = 100$, $E = 1.0$ GeV. The cut-off becomes even sharper at higher values of E.

and corresponds to 0.045 GeV in these figures. The transverse momenta of the photons is then calculated according to

$$\frac{\int_0^{p_\perp} dp'_\perp \frac{dN(E,p'_\perp)}{dp'_\perp}}{\int_0^{1.5/R} dp'_\perp \frac{dN(E,p'_\perp)}{dp'_\perp}}$$

where $\int N(E,p_\perp) \equiv \int_0^{p_\perp} dp'_\perp \frac{dN(E,p_\perp)}{dp_\perp}$ can be computed analytically as

$$\int N(E,p_\perp) = e^{-u_0}\left[\frac{e^{-u_1}}{1+u_1/u_0} - 1\right] + (u_0+1)\left[\ln(1+\frac{u_1}{u_0}) + \sum_{n=1}^{\infty}\frac{(-1)^n\left((u_0+u_1)^n - u_0^n\right)}{(n)n!}\right] \tag{14}$$

where $u_0 \equiv 2\left(\frac{ER}{\gamma}\right)^2$ and $u_1 \equiv 2(p_\perp R)^2$. Although twenty terms of the Taylor expansion must be retained in order to give sufficient accuracy for the range of $p_\perp < 1.5/R$ and $E < 1.5\gamma/R$, this approach is useful; otherwise the table would have to be recalculated at each value of E. The $p_\perp$ of the $\gamma\gamma$ system is the sum of the $p_\perp$ of the two individual photons, added together using randomly chosen angular separation.

The mesons in Table 1 decay strongly. To simulate the decays, it is necessary to consider the meson spins. Two real photons can combine to form either spin 0 or spin 2 final states. The spin 0 final states decay isotropically, while the spin 2 states are oriented along the beamline and decay with a $\sin^2\theta$ angular distribution where θ is the angle between the beam and the decay in the $\gamma\gamma$ rest frame. The former can be handled by standard decay routines in JETSET; the latter must be included explicitly in the Monte Carlo. The azimuthal angle for each decay is assigned randomly, and the $\gamma\gamma$ system boosted into the lab frame, and p_x, p_y and p_z found, following the standard STAR coordinate system.

Because of the need to include spin effects explicitly, only a limited subset of the mesons in Table 1 is currently included in the Monte Carlo: $f_0(975) \rightarrow \pi^+\pi^-$, $\eta_c \rightarrow K^{*0}K^-\pi^+$, with $K^{*0} \rightarrow K^+\pi^-$, and $f_2(1270) \rightarrow \pi^+\pi^-$. The η_c is decayed using JETSET, so other final states could be easily generated. In the future, we plan to integrate the STARlight photon generator with a more general $\gamma\gamma$ Monte Carlo.

For muon and tau pairs, the situation is more complicated. The angular distribution for lepton pairs in the center of mass frame is given in Brodsky[6]

$$G_{\mu^+\mu^-}(\theta) = 2 + 4\left(1 - \frac{4m^2}{W^2}\right)\frac{\left(1-\frac{4m^2}{W^2}\right)\sin^2\theta\cos^2\theta + \frac{4m^2}{W^2}}{\left(1-\left(1-\frac{4m^2}{W^2}\right)\cos^2\theta\right)^2} \tag{15}$$

where m is the lepton mass, and θ is the angle between the beam and the decay in the center of mass frame of the system. A table generated from this distribution is used to compute center of mass momenta which are then boosted into the lab frame. Hadron pairs will also be forward peaked, but the distributions will change somewhat depending on the exact final state.

For tau pairs, there is an added complication in that the taus decay quickly. First the angular distribution of the taus in the center of mass frame is calculated using a table based on Equation 15. These results are then boosted into the lab frame in a manner similar to the muons. Then, each tau is allowed to decay. The decay channels considered for the taus are

$$\tau^+ + \tau^- \rightarrow \ell^+ + \nu_\ell + \bar\nu_\tau + \ell^- + \bar\nu_\ell + \nu_\tau$$

where the ℓ's are either muons or electrons. Both the electrons and muons are treated as massless, allowing the energy distribution to be expressed in the tau center of mass frame as[13]

$$\frac{d\Gamma}{dE} \propto E^2 \left(1 - \frac{4E}{3m_\tau}\right). \tag{16}$$

where E is the energy of the charged lepton. The energies of the final state charged leptons are calculated by using a normalized table of the integral of this function. The angular distribution of these leptons is calculated by first randomly choosing the spin of one of the taus in the direction of the beam (s_{τ_1}). As the photon initial state must be spin zero to decay to produce taus, $s_{\tau_2} = -s_{\tau_1}$. The direction of ℓ_1 and ℓ_2 were then assigned according to

$$f(\omega) = 1 + \frac{1}{3}\cos(\omega) \tag{17}$$

where ω is the angle of the particle with respect to the direction along which spin is assigned. Azimuthal angles were randomly assigned to each of the ℓ's and each particle is then boosted according to the tau from which it decayed. While the directions of the leptons are correlated, in the $\gamma\gamma$ center of mass frame the overall distribution of charged leptons is isotropic. This approach preserves the proper angular correlation between ℓ_1 and ℓ_2.

Rho pairs are decayed using a simpler model, ignoring spin and assuming that pairs are produced with negligible momenta in the center of mass frame. This is appropriate only near threshold. Each ρ is then decayed into a $\pi^+\pi^-$ pair with a random orientation in the center of mass frame.

This Monte Carlo code is available to all members of the STAR collaboration. Documentation can be found at http://rsgi01.rhic.bnl.gov/star/starlib/doc/www/html/ssd_l/stl_l/stl.html web page which is linked to the simulation documentation page. The code is available on request, and will be re-installed shortly. The type of colliding ions and γ values are input parameters. Each output event includes the number of final state particles, decay number, particle id's and four momenta. STARlight can produce output formatted for the current STAR GEANT or the new Gstar; the latter retains interior vertex information.

6 STAR Acceptances

Using this Monte Carlo, we conducted a preliminary study of STAR acceptances using 250,000 events of each type. Events were analyzed using simple criteria to determine if the particles would be seen in the STAR TPC or FTPC.

A particle was considered to have hit in the TPC if $|\eta| < 2$ and $p_\perp > 150$ MeV/c. The $p_\perp$ cut ensured that the tracks would hit the trigger detectors. A particle was considered to have hit the FTPC if it had $2.5 < |\eta| < 4$ and $p_\perp > 50$ MeV/c. The FTPC $p_\perp$ cut is a crude but conservative estimate based on the material in the beampipe as a function of angle, and the magnetic bending. Because of the preliminary state of the FTPC design and probable lack of an FTPC trigger, the FTPC is used mostly as a veto here. Physics analyses where it would be a primary detector, mainly diffractive pair production, are postponed until the FTPC design is at a more advanced stage.

Decay	All TPC	1TPC 1FTPC	2 FTPC	Branch. Ratio	Evts/ year
$\mu^+\mu^-$	7.5 %	2.0 %	1.7 %	—	4.7 / s
$\tau^+\tau^- \to$ leptons	61 %	9.4 %	0.72 %	13 %	150
$f_0(975) \to \pi^+\pi^-$	75 %	7.4 %	0.36 %	52 %	1.2×10^5
$f_2(1270) \to \pi^+\pi^-$	85 %	4.2 %	0.07 %	56 %	9.2×10^5
$\rho^0\rho^0 \to \pi^+\pi^-\pi^+\pi^-$	38 %	—	—	—	1.6×10^4
$\eta_c \to K^{*0}K^-\pi^+ \to K^+\pi^-K^-\pi^+$	57 %	—	—	1.67 %	70

Table 3: Acceptances and expected rates for accepted events at STAR for gold beam collisions, for decay products hitting the TPC and/or FTPC. The number of events per year is calculated using the rates in Table 2.

While the TPC and FTPC detection criteria are fairly crude, they are adequate for determining signal to noise ratios. If one wanted to improve tracking by, for example, only using TPC tracks with $|\eta| < 1.5$, the signal would be reduced, but so would the background. At this point, we have neither the manpower nor the computer power to run large samples of $\gamma\gamma$ and background events through the entire STAR simulation and reconstruction programs.

From these criteria, acceptances for all particles in the TPC, one in the TPC and one in the FTPC, and two particles in the FTPC were obtained. These are given in Table 3 along with branching ratios to the decay channels we examined and expected number of measured events per year. The fraction of events measurable is based only on events where all particles are detected in the main TPC; including the FTPC would raise these numbers slightly.

7 Backgrounds

There are four major backgrounds that need to be considered: peripheral nuclear collisions, beam-gas interactions, photon-nucleus collisions, and Pomeron processes. Peripheral nuclear collisions and beam-gas interactions can be simulated with FRITIOF and VENUS. The latter two backgrounds are of considerable physics interest.

Unfortunately, no Monte Carlo for photon-nucleus interactions currently exists. Existing γp Monte Carlos are unsuitable even for a first pass because they use a photon spectrum that is wildly inappropriate for RHIC conditions. Although the cross section for γN interactions is large, in most cases the reaction products will go down the beampipe. However, because of the lack of a Monte Carlo, rate calculations remain to be done. Many of the cuts used to reject beam-gas interactions should be useful in separating photon-nucleus collisions from $\gamma\gamma$ interactions.

The final 'background', from coherent Pomeron-Pomeron and Pomeron-photon interactions, is sufficiently similar to photon-photon interactions that these interactions can at best be separated statistically. Because Pomerons are of considerable physics interest themselves, they can only make the physics more interesting. Of special interest is the fact that RHIC is the first place where it might be possible to investigate interference between photon and Pomeron mediated interactions.

This note will examine the remaining backgrounds: peripheral nuclear collisions and beam-gas reactions. Cosmic ray muons will be discussed in the section on triggering, but are not expected to be a significant background for analyses.

The backgrounds are reduced with a series of cuts that exploit the characteristics of $\gamma\gamma$ events. While the exact cuts must be tailored to a specific analysis, certain cuts are generally useful. The analyses considered here are restricted to final states containing two or four charged particles, and no photons. Since we are only interested in events that are fully reconstructed, we can immediately require two or four charged particles in the TPC, no charged particles in the FTPC, and no photons in the calorimeter. The charged particles must have a net charge zero. This charged and neutral multiplicity is much lower than that of the expected backgrounds. A second general cut concerns perpendicular momentum of the final state system, taken as a whole; because the photons couple coherently to the entire nucleus, the perpendicular momentum scale for each photon is smaller than 1/R, the nuclear size, or about 30 MeV/c for gold. This compares with a few hundred MeV for typical hadronic interactions. Even though the individual final state particles may have $p_\perp > 100$ MeV/c, $\Sigma p_\perp$ should be small. So, requiring that $\Sigma p_\perp < 100$ MeV/c will greatly reduce the background, with minimal loss of signal. Many other cuts are useful, but are analysis specific, and are discussed in the following section.

Peripheral nuclear and beam-gas interactions were studied using the FRITIOF[18] and Venus[28] Monte Carlos. To study the effects of peripheral nuclear collisions, 247,627 FRITIOF and 37,055 Venus events were generated for gold beam collisions with impact parameters ranging from 12 to 18 fm. This range was found by trial and error to correspond to that which can produce low multiplicity collisions in the TPC. Figure 6 shows normalized impact parameter histograms of events with TPC multiplicities of 1-6 for both gold on gold and beam-gas events. These histograms show that the full range of impact parameters contributing to low multiplicity events has been considered. The geometric cross section corresponding to this range of b is 5.6×10^{-24} cm^2, which gives a base geometrical reaction rate of 1,100 Hz.

The background estimates presented here should be accurate to a factor of $2-5$. This estimate is based on the differences between FRITIOF and Venus predictions. While FRITIOF and Venus agree fairly well on some basic parameters, such as the overall rates for low multiplicity events, the differences are large in the specific analyses. The reasons for the difference are unclear, but part of the difference appears to stem from differences in some resonance production rates. It is probably worth pointing out here that, even in the most pessimistic background estimates, the signal to noise ratios are suitable for doing much good physics. It is also worth noting that the differences between FRITIOF and Venus are large enough that peripheral collisions may be useful in tuning the codes.

Statistical errors, while large, are small compared to this systematic uncertainty. Even with 250,000 (37,000) events, corresponding to almost 4 minutes (30 seconds) of RHIC running for FRITIOF (VENUS), the background statistics are marginal for many analyses, and various extrapolations must be used to improve the statistics. The accuracies of these extrapolations should be considerably better than the uncertainties from the physics (Monte Carlo) models. Compared with these uncertainties, the simple detector models used here do not contribute significant error.

The residual gas in the beam line was modeled as ionized hydrogen at 1.0×10^{-9} torr. This is a reasonably conservative number; the RHIC conceptual design report predicts that

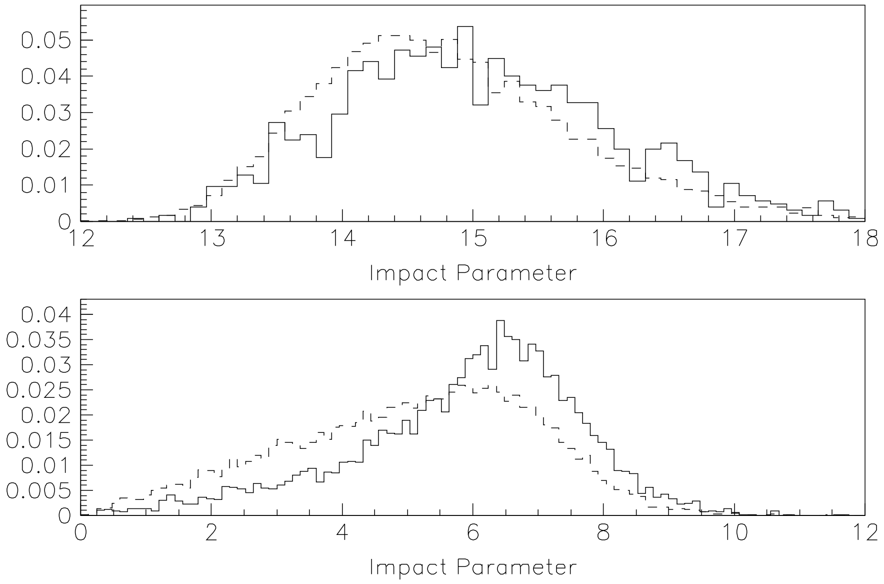

Figure 6: Normalized impact parameter histograms of events with TPC multiplicities of 1-6. The upper plot is for gold on gold collisions, and the lower plot is for beam-gas events. The solid curves are from Venus and the dashed lines are from FRITIOF.

pressures in the warm section of the beamline will be less than 1×10^{-10} torr [10] at a temperature of 273^oK. K. Welch estimated[27] that, in the most probable bakeout scenario, the average 8×10^{-10} torr, with the maximum pressure in the center of the beam pipe less than 1.5 times that. The worst scenario that he considers 'possible' is still under 10^{-9} torr average pressure. While these numbers will depend on the exact details of the beampipe size, composition and bakeout, if they hold up, then beam-gas is not a major problem.

Beam-gas collisions were examined by generating 38,640 FRITIOF and 16,000 Venus gold on stationary proton events with impact parameters less than 18 fermi for FRITIOF and 11.8 fermi for Venus. This difference was due to an upper bound set by Venus. For analysis studies, we accept events occurring ± 20 cm of the center of the detector (for triggering studies this requirement is relaxed); if beam-gas is a problem, this cut could be tightened somewhat with little loss of luminosity. These parameters result in base geometrical reaction rates of 125 Hz for FRITIOF and 55 Hz for Venus.

The Monte Carlo events were analyzed in a similar manner in which the acceptances were calculated. This section discusses general analysis techniques which are applicable to a wide range of studies; the following section considers three specific analyses which use these techniques.

As before, a TPC hit was defined as $|\eta| < 2$ and $p_\perp > 150$ MeV/c, and an FTPC hit was defined as $2.5 < |\eta| < 4$ and $p_\perp > 50$ MeV/c. In addition, the calorimeter is used for background rejection. Photons were considered to be detected in the electromagnetic calorimeter if they had energies > 100 MeV and $-1 < \eta < 2$. The asymmetric η cut is because the calorimeter is expected to include only one endcap.

We have not performed a detailed study of the backgrounds without the electromagnetic calorimeter. However, Table 4 shows rates for various categories with one photon present as well as with no photons. Since isospin symmetry predicts $N_\gamma \approx N_{charged}$, backgrounds without the calorimeter should be at most a few times the backgrounds with neutral particle rejection; Figure 4 predicts a lower increase. In fact, the situation is considerably better than this because the analysis places requirements on the perpendicular momentum of the system. Events with a missing photon will, on the average, have a higher observed perpendicular momentum, and hence be preferentially rejected by this cut. This is why photons outside the calorimeter acceptance are also under control.

The results of the analysis are summarized in Table 4. "Number of tries " is the number of times that two ions passed each other within the specified range of impact parameters. From these crossings, the Monte Carlo generated an interaction only for the number of events given as "Collisions." From these collisions, we count the number of events in which two or four particles are detected in the TPC, with 0 or 1 photon detected in the electromagnetic calorimeter. The $\gamma\gamma$ system has charge zero, so events reconstructed with charge 2 can be rejected. As the transverse momentum of the $\gamma\gamma$ system is small, $\sim 1/R \sim 45$ MeV/c, as was shown in Figures 4 and 5, a cut of $\Sigma p_\perp < 100$ MeV/c can be made, resulting in values close to the limit of what can be considered given the available statistics. The 100 MeV/c $p_\perp$ cut is actually fairly loose, to allow for event reconstruction errors, but could be tightened up where background is a problem.

Finally, Table 4 also includes the fraction of events in which at least one track was found in the FTPC. To improve statistics, this was calculated using all events with TPC multiplicities between 1 and 6. These high rejection rates indicate that the FTPC will be important as a veto in reducing peripheral ion collisions and beam-gas events. Such a veto detector need not provide as much information as the FTPC, and a simple scintillator detector would be equally as effective if the FTPC is not yet present. These results also suggest that covering the region of $2 < |\eta| < 2.5$ with scintillator would provide an additional veto, but only if machine related backgrounds are low.

As an example of the effectiveness of the perpendicular momentum cut, Figure 7 compares the $p_\perp$ of background events with the $p_\perp$ of the $\gamma\gamma$ system for production of ρ pairs near threshold (1500-1600 MeV). The number of events in this plot have been normalized to values after 10^7 seconds running. The total number of ρ pairs detected is thus taken to be 16,000 as in Table 3. The other two curves were calculated from FRITIOF data for multiplicity 2 and events with 0 or 1 photon in the calorimeter. They are normalized to represent only the number of events with multiplicity 4, $\Sigma Q = 0$, no photons, and no tracks in the FTPC.

8 Sample Analyses

To better understand background rejection, we have conducted sample analyses for three representative signals. In these analyses we systematically applied cuts appropriate for examining a certain type of event, and compared the number of background events to expected number of signal events to calculate a signal to noise ratio.

The first analysis was for resonances with masses greater than ≈ 1 GeV which decay to two-particle final states. Specifically, we examined resonances which decay to $\pi^+\pi^-$ such as the $f_0(975)$ and the $f_2(1270)$ but the analysis should be similar for other two-particle final states such as $f_2(1525) \to K^+K^-$.

To extract this signal from the background, we first required that that two-particle final

Number	Peripheral Ion Collisions		Beam-Gas Collisions	
	FRITIOF	Venus	FRITIOF	Venus
Number of tries	247,628	37,055	229,291	43,536
Geometric Rate	1,100 Hz	1,100 Hz	125 Hz	55 Hz
Collisions	105,239	16,580	38,640	16,000
Corresponding Rate	470 Hz	490 Hz	21 Hz	20 Hz
Mult 2, 0 photons	496	36	2,630	1,255
Mult 2, 1 photon	296	34	2,780	1,220
Mult 4, 0 photons	164	31	375	240
Mult 4, 1 photon	260	36	382	225
ΣQ = 0 and				
Mult 2, 0 photons	354	26	1,480	723
Mult 2, 1 photon	208	24	1,675	662
Mult 4, 0 photons	119	19	194	121
Mult 4, 1 photon	157	24	197	113
ΣQ = 0, $p_\perp < 100$ MeV and				
Mult 2, 0 photons	30	3	112	37
Mult 2, 1 photon	14	0	108	26
Mult 4, 0 photons	0	2	12	1
Mult 4, 1 photon	3	0	7	0
FTPC hit	96%	90%	94%	90%

Table 4: Expected background rates for peripheral nuclear and beam-gas collisions, for the FRITIOF and Venus Monte Carlos. The initial rates and the results of various cuts are shown. The first cuts require multiplicity 2 or 4 in the main TPC, 0 or 1 photon in the calorimeter. The second group also requires that the final state have a total charge zero, and the third group additionally requires that the perpendicular momentum of the detected system be less than 100 MeV/c.

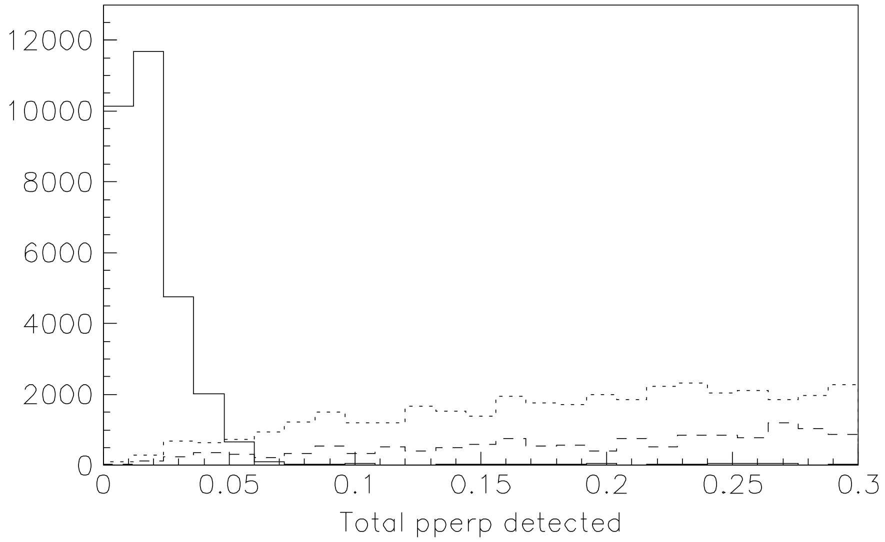

Figure 7: Comparison of perpendicular momentum between $\gamma\gamma$ and background events. The solid curve gives $p_\perp$ of the $\gamma\gamma$ system for production of $\rho^0\rho^0$ near threshold (1540 MeV). The short dashes are for beam-gas events and the long dashes are for peripheral nuclear events. Both background are for 4π masses in the 1.5 to 1.6 GeV range, multiplicity 4, $\Sigma Q = 0$, no detected photons, and no particles in the FTPC. All curves are normalized to the number of events per year (10^7 seconds) running.

state be charge neutral, with no photons detected in the EM calorimeter. This lowered the background predicted by each of the Monte Carlos to those given in the first row of Table 5. The table gives the number of events per year (10^7 seconds) of running and is calculated from the data shown in Table 7.

Next, events were required to have total $p_\perp < 100$ MeV/c. At this point the background samples ran out of statistics. To make further cuts, these numbers are reduced based on percentages assume based on larger data sets. This is only correct if the cuts are independent. While not strictly true, the errors introduced by this assumption should be much smaller than the FRITIOF-Venus difference.

By comparing the total number Mult 2, $\Sigma Q = 0$, no γ, events with those with invariant mass > 1 GeV, we estimate the total number of events passing an invariant mass cut for each type of background. The numbers which were used to calculate these rates appear at the end of the section in Table 8. Plots of invariant mass appear in Figure 8.

Finally, a cut was made allowing no charged particles to be found in the FTPC. The effect of this cut was estimated by using the rejection rates given at the end of Table 7. These were calculated using the full sample of each type of event.

Summing the remaining backgrounds from hadronic and beam-gas events, FRITIOF predicts $18,000$ two-particle background events with Mass > 1 GeV per year, while Venus predicts that there will be $26,000$ of these events per year. These numbers can be compared with $f_0(970)$ and $f_2(1270)$ production rates of 120,000 and 920,000 events per year respectively, after acceptance cuts. As the invariant mass cut can be further constrained depending on the exact particle which is being considered, these ratios indicate that measurement of

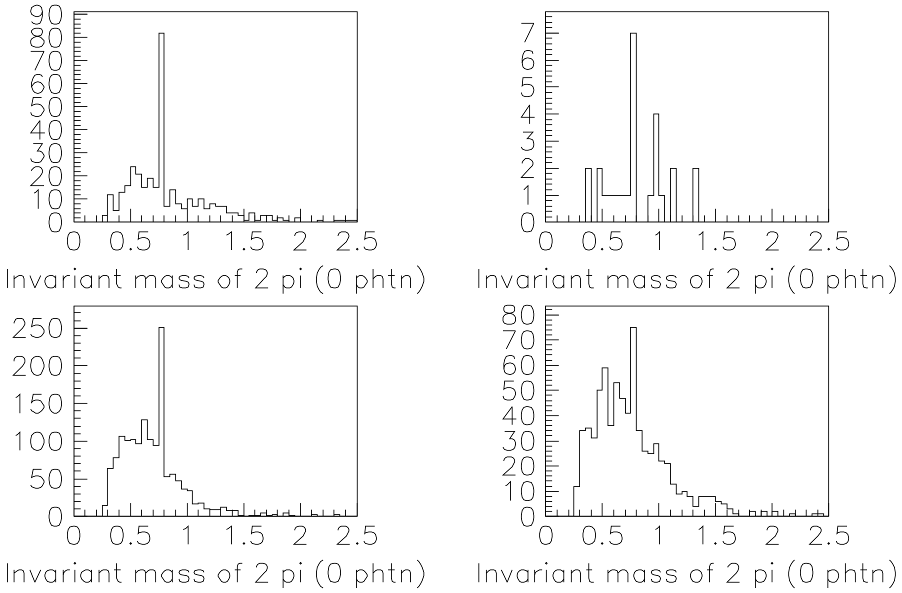

Figure 8: Invariant masses of charge neutral background events with two tracks in the TPC and no photons in the EM calorimeter. The upper plots are peripheral collisions and the lower curves are beam-gas events. FRITIOF events are on the left and Venus on the right. The peak at about 750 MeV is from ρ^0 decays. The ρ^0 peak is so narrow because the FRITIOF does not include it's width.

Cuts	Peripheral Ion Collisions		Beam-Gas Collisions	
	FRITIOF	Venus	FRITIOF	Venus
Mult 2, $\Sigma Q = 0$, 0 photons	16 M	7.7 M	8.1 M	9.1 M
$p_\perp < 100$ MeV	1.3 M	900 K	610 K	470 K
Invariant Mass > 1 GeV	340 K	170 K	68 K	88 K
FTPC cut	14,000	17,000	4,100	8,800

Table 5: Expected backgrounds for particles decaying to two charged particles. These cuts are loose, appropriate to a multi-parameter phase shift analysis. For individual particle searches, the mass cut could be greatly tightened, further reducing the backgrounds. All rates are given for 10^7 seconds of running. K=1,000 and M=10^6.

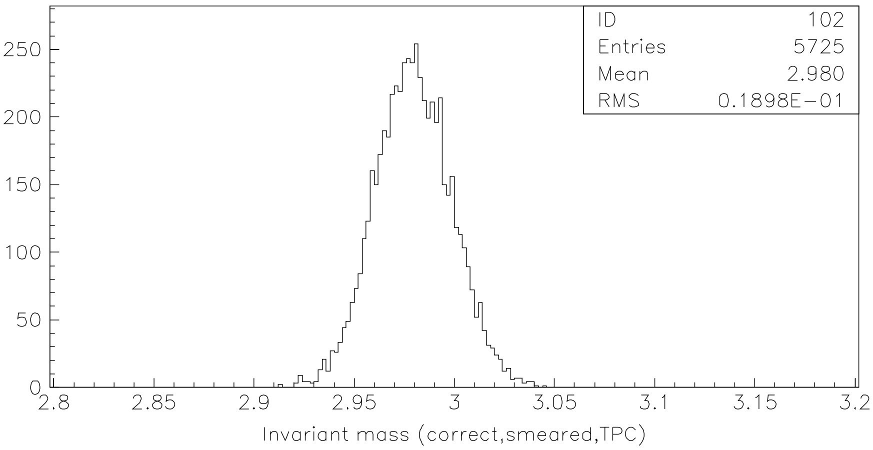

Figure 9: Plot of reconstructed invariant mass of η_c events with momenta smeared to model the TPC only resolution.

these and similar particles should be possible at STAR. In fact, the backgrounds for all two charged pion final states should be low, allowing for angular analyses to be performed.

The next analysis was the measurement of the $\gamma\gamma$ width $\Gamma_{\gamma\gamma}$ of the η_c, seen through the decay channel $\eta_c \rightarrow K^{*0}K^-\pi^+ \rightarrow K^+\pi^-K^-\pi^+$. Because the η_c is narrow, the width of the observed η_c mass peak is dominated by detector resolution. The detector resolution was studied with 10,000 η_c decays which were generated using STARlight. Events where all final state particles were detected in the TPC were selected. For these events, the particle momenta were smeared to simulate the resolution of the TPC and of the TPC+SVT.

In both the TPC and TPC + SVT models, the p_x, p_y, and p_z of each track was randomly smeared according to a Gaussian distribution with a width determined by the $p_\perp$ of the particle. For the TPC: $\frac{\Delta p}{p} = 2\%$ if $p_\perp < 200$ MeV, $\frac{\Delta p}{p} = 1.5\%$ if 200 MeV$< p_\perp < 1$ GeV, and $\frac{\Delta p}{p} = 0.5\% + 1\%/\mathrm{GeV}$ if $p_\perp > 1$ GeV. For the TPC+SVT, $\frac{\Delta p}{p} = 2\%$ if $p_\perp < 200$ MeV and $\frac{\Delta p}{p} = 1.4\% + 0.1\%/\mathrm{GeV}$ if $p_\perp > 200$ MeV. These numbers were based on plots in the STAR Conceptual Design Report [25]. Because this assumes that the tracking is optimum even in the region $1 < |\eta| < 2$, it is optimistic, but probably by less than a factor of two.

After the momenta were smeared, the invariant mass of the event was calculated, assuming that the kaons and pions were correctly identified. A plot of the invariant mass distribution obtained from the TPC only model is given in Figure 8, which indicates a standard deviation of ≈ 20 MeV. The TPC + SVT model leads to a similar plot, with a standard deviation of $18.6 \approx 20$ MeV

Using this width, the expected backgrounds to an η_c search are given in Table 5. Considering charge neutral events with multiplicity 4 and 0 photons, a cut of $p_\perp < 100$ MeV was applied as it was in the two-particle case. For the four particle $p_\perp$ cuts, limited statistics required the use of both 0 and 1 photon events in the calculation of the percentage of events passing this cut.

Also due to low statistics, the invariant mass cut was calculated using both 0 and 1 photon data, using the region within ± 100 MeV of 3.0 GeV and scaling down to $\pm 2\sigma = 40$ MeV. The FTPC cut was again modeled using the percentages at the end of Table 7. Plots of the invariant mass of 4 track charge neutral events with no photons are given in Figure

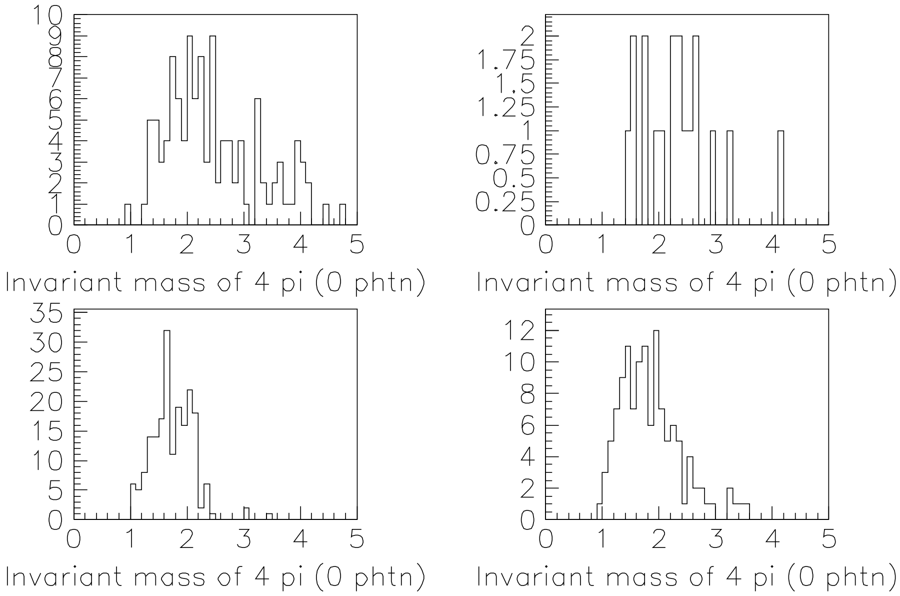

Figure 10: Invariant masses of charge neutral background events with 4 tracks in the TPC and no photons in the EM calorimeter. The upper plots are peripheral collisions and the lower curves are beam-gas events. FRITIOF events are on the left and Venus on the right.

Cuts	Peripheral Ion Collisions		Beam-Gas Collisions	
	FRITIOF	Venus	FRITIOF	Venus
Mult 4, $\Sigma Q = 0$, no photons	5.2 M	5.6 M	1.1 M	1.5 M
$p_\perp < 100$ MeV	57 K	260 K	51 K	6.4 K
Invariant Mass $= 3 \pm 0.040$ GeV	910	4,800	300	33
FTPC cut	36	480	18	3.3

Table 6: Expected backgrounds to a search for $\eta_c \to K^{*0}K^-\pi^+$, for 10^7 seconds of running.

10.

As Table 6 shows, FRITIOF predicts 54 background events per year while Venus predicts 480 events. These can be compared to an expected signal of 70 events per year. Further background rejection may be attained by using dE/dx and TOF to identify the two charged kaons in the final state. If 10% of the background tracks are kaons, and particle identification can reject 80% of the pions, then a rejection factor of 5 per kaon can be obtained, or 25, leaving backgrounds of 3 or 20 events per year. An additional small factor could be obtained by requiring that one of the $K\pi$ pairs fit a K^{*0} mass hypothesis. If the statistics are still marginal, it will be possible to sum signals from several different η_c decay channels, increasing the statistics by a factor of a few, and allowing a rate measurement. While these numbers sound fairly promising, determining the actual feasibility of this measurement will probably have to await initial data.

The final analysis is the measurement of ρ^0 pairs near threshold, decaying to 4 charged pions. Because the ρ pair production is continuous and the ρ peak is wide, mass resolution is of little relevance. This analysis accepted all events with four charged particles, assumed to be pions, with an invariant mass in the 1.5-1.6 GeV threshold region. Otherwise the analysis

Cuts	Peripheral Ion Collisions		Beam-Gas Collisions	
	FRITIOF	Venus	FRITIOF	Venus
M 4, $\Sigma Q = 0$, 0 γs $p_\perp < 100$ MeV	57 K	260 K	51 K	6.4 K
Invariant Mass = 1550 ± 50 MeV	2,200	9,100	6,100	490
FTPC cut	88	910	366	49

Table 7: Expected backgrounds to a study of $\rho^0\rho^0$ production near threshold.

Number	Peripheral Ion Collisions		Beam-Gas Collisions	
	FRITIOF	Venus	FRITIOF	Venus
Mult 2, 0 photons	354	26	1,480	723
Mult 2, 1 photon	208	24	1,675	662
Mult 4, 0 photons	119	19	194	121
Mult 4, 1 photon	157	24	197	113
Mass > 1 GeV and				
Mult 2, 0 photons	91	5	165	135
Mult 2, 1 photon	46	4	143	93
Mass 3.00 $\pm$0.04 GeV and				
Mult 4, 0 photons	2.0	0.4	0.8	0.4
Mult 4, 1 photon	2.4	0.4	1.6	0.8
Mass 1.5-1.6 GeV and				
Mult 4, 0 photons	4	0	27.5	10
Mult 4, 1 photon	6.5	1.5	19.5	8

Table 8: Summary of the Monte Carlo rates used to make mass cuts for charge 0 events. For the η_c, the number of events was calculated by examining values within 100 MeV and scaling appropriately.

of this decay proceeded exactly as that of the η_c. Again, both 0 and 1 photon data were used in computing $p_\perp$ and invariant mass cuts, and we considered the range of invariant masses with $\pm$100 MeV of 1550 MeV and scaled appropriately. FTPC cuts were computed as in Table 7. The results of this analysis appear in Table 7.

For this decay FRITIOF predicts 450 background events per year while Venus predicts 960. These numbers suffer from same low statistics as in the η_c analysis. Comparing these numbers to an expected signal of 16,000 events per year, however, indicates that even if these numbers are an order of magnitude off, measurement of ρ pairs should be possible with STAR.

For all of these analyses, the backgrounds can be accurately measured by considering events with 100 MeV/c< $p_\perp$ < 200 MeV/c, as suggested by Figure 7.

By using a small number of cuts (multiplicity, ΣQ, number of photons, $\Sigma p_\perp$, invariant mass, and FTPC hits) analysis of many different final states should be possible. The $f_0(975)$, $f_2(1270)$ and similar particles should be measurable with STAR as will ρ pairs near threshold. The η_c rate may be measurable, but this may depend on the use of particle identification.

9 Triggering

To be able to do any of these analyses, STAR must be able to trigger on low multiplicity events without being overwhelmed by backgrounds. In addition to the previously mentioned backgrounds, cosmic ray muons passing through the TPC can mimic two-track events. During analysis, these muons are easily rejected by requiring that the reconstructed tracks pass through the expected interaction diamond, but at trigger Levels 0-2, they could be a problem. While we have obtained a cosmic ray muon Monte Carlo, it is not yet integrated with STAR software[5]. Instead, crude rate estimates will be discussed at the end of this section.

Trigger rates from glancing nuclear and beam-gas events were studied using the previously described Monte Carlo samples. The absence of primary vertex information at trigger Levels 0-2 (the VPD is not useful in low multiplicity collisions), introduces an additional complication for beam-gas events. Beam-gas events can occur anywhere along the beampipe. Without vertex information, collisions anywhere in the beampipe must be considered. For events significantly outside of STAR ($|z| > 2$ meters), the endcaps will shield the MWPC and CTB slats, so they will not be considered here. Because the beampipe vacuum is better far from the interaction region, and because outside of STAR, the endcaps will provide shielding for the MWPC and CTB slats, the region $|z| > 2$ probably contributes considerably less than the central region. This is within the factor of two systematic error discussed previously.

Because of the varying vertex position, the TPC and calorimeter angles can no longer be modeled simply using pseudorapidity. The angles from the actual interaction point to the CTB and endcaps must be considered.

A position z_{vertex}, and a direction d were randomly assigned to each event, such that $0 < z_{vertex} < 4$m and $d = \pm 1$. A TPC hit was then defined as $p_\perp >$150 MeV/c and $0 < z_{vertex} + 0.5\text{m} \times \text{d} \sin(\theta) < 4$m. An EMC hit was defined as $0 < z_{vertex} + 2.0\text{m} \times\text{d} \sin(\theta)$ and $z_{vertex} + 0.5\text{m} \times\text{d} \sin(\theta) < 4$m where θ is the angle between the particle track and the beamline. Using these definitions, we were able to apply successive cuts and estimate backgrounds at each level of the trigger. A summary of this analysis appears in Table 9.

To calculate rates at each trigger level, it is necessary to consider the available information. At Level 0, the only usable information available is crude charged particle multiplicity using the CTB and MWPC coarse pixel array. As a single particle can hit more that one wire in the endcaps or more than one detector in the trigger barrel, we allow a loose Level 0 trigger of 1-5 particle multiplicities. The rates are summarized in Table 9; the rate is about 45 Hz from peripheral collisions and 150 Hz from beam-gas events. If calorimetric information is available, these rates could be reduced.

Because of uncertainties as to when the EMC trigger information becomes available, it isn't clear what can be done in Level 1 and what must wait until Level 2, so both levels will be lumped together here. At least three additional cuts can be made. First, when EMC information is available, events containing photons can be rejected. Second, at Level 2, when detailed slat/wire multiplicity information becomes available, we can more accurately count multiplicity, and require multiplicity exactly 2 or 4. Third, for two-track events, we can require that the two tracks be roughly azimuthally back to back; here we require that the angle between the two tracks be greater than 150 degrees. For four charged particles, there is a similar requirement, that there does not exist a line in the xy plane such that all four particles lie on one side of it. These cuts reduce the Level 2 output rate to about 20 Hz,

Number	Peripheral Ion Collisions FRITIOF	Peripheral Ion Collisions Venus	Beam-Gas Collisions FRITIOF	Beam-Gas Collisions Venus
Level Zero				
1-5 TPC Hits	48	39	151	155
Level One/Two				
Mult 2, 0 photons	2.1	1.1	17.7	18
Mult 2, 0 or 1 photon	3.5	2.1	29.7	30
Mult 4, 0 photons	0.8	0.9	9.0	9
Mult 4, 0 or 1 photon	1.9	1.9	13.6	13
Angular cuts and				
Mult 2, 0 or 1 photons	1.0	0.5	7.2	7.0
Mult 4, 0 or 1 photons	1.2	1.2	8.8	8.0
Level Three				
Angular Cuts, $\Sigma Q = 0$ and				
Mult 2, 0 or 1 photon	0.7	0.4	4.6	4.3
Mult 4, 0 or 1 photon	0.7	0.8	4.2	3.6
$\Sigma Q = 0$, vertex localized,				
0 or 1 γ's and $p_\perp < 0.1$ GeV				
Mult2	0.19	0.09	0.12	0.08
Mult4	0.013	0.06	0.010	0.002

Table 9: Summary of expected trigger rates due to background, for Levels 0 to 3, calculated by level. All values are in Hz.

about 80% of it from beam-gas events. All of these cuts are quite simple, and a Level 1/2 decision can hence be made quite quickly after a processor is assigned, producing quick TPC aborts when desired.

At Level 3, TPC tracking is available, allowing for many more cuts to be used. First, the primary vertex can be found, and beam-gas events outside the $\pm 20cm$ diamond can be rejected. Second, with tracking, charge information is available, so a total charge zero requirement can be imposed. Finally, a perpendicular momentum cut can be imposed. As Table 9 shows, these cuts should reduce the background rates to less than 1 Hz. This is considerably less than the trigger rate due to $\gamma\gamma \rightarrow \mu\mu$, so any further attempts to reduce the rates will inevitably lead to a loss of signal.

Because these events are very small, less than 1% of the size of central gold-gold collisions, they should impose little load on the DAQ system. The DAQ system is designed to write out small, calorimeter only pp events at high rates; the same scheme could be used here. Having said that, effort is required to insure that this capability is indeed available for low multiplicity TPC events.

The major remaining concern for triggering is cosmic ray muons. The raw rate for cosmic ray muons hitting the TPC (modeled as a 4 meter long, 2 meter radius cylinder) is about 2 kHz. The mean energy is about 2 GeV. Shielding above the TPC will reduce the rate significantly. Shielding comes from the detector hall roof (3 feet of concrete, 229 g/cm^2), magnet coil (about 34 cm thick, 60% coverage (the rest is cracks); averaging 55 g/cm^2 of aluminum) magnet steel (24 inches thick, about 70% coverage, averaging 336 g/cm^2 of iron), and the calorimeter, another 110 g/cm^2. The total thickness is 730 g/cm^2, enough to stop 1.5 GeV vertically incident muons (higher for off-zenith muons). The shielding stops about 40% of the muons, reducing the rate to 1.2 kHz. Because the CTB ADC gates are planned to be open for 40 nsec out of the 105 nsec RHIC crossing interval, the rate to produce Level 0 triggers drops to 460 Hz, and would be lower if the ADC gate can be shortened. In addition, the magnetic field in the iron (which should be saturated) will provide substantial bending of muons, and reduce the rates significantly. Finally, the two hit requirement in the CTB + MWPC limits the geometric aperture, especially if the hits must be roughly back to back. Together, these requirements may reduce the rate to an acceptable level.

If the rate is too high, two methods could be used to reduce it. The first would be to eliminate nearly vertical back to back events. If this is needed at Level 0 where only coarse pixel information is available, considerable signal would be lost. If it can wait until Level 2, when slat-by-slat information is available, the loss would be much less.

Alternately and preferably, timing information from the CTB could be used to reject out of time two-track events, This would require some additional TDCs. Alternately, a TDC connected to a piece of scintillator atop the detector might be usable, if backgrounds are low enough. Either approach should provide enough cosmic ray rejection to keep the trigger rates low.

A detailed study of cosmic ray muon rates is required soon.

10 Conclusions

Two-photon physics is an interesting new physics topic for STAR. Because of the large nuclear charge, below 1.5 GeV, RHIC will have the highest $\gamma\gamma$ luminosity available anywhere, generating many interesting final states at high rates. Although the STAR detector was not designed for low multiplicity events, it is quite well suited for the job.

Our studies indicate that the backgrounds are relatively small, and the expected trigger rates are easily manageable. Nevertheless, expected backgrounds due to photon-nucleon interactions require Monte Carlo study, along with cosmic ray muons. The RHIC vacuum will also require some watching. In addition, the interplay between photon and Pomeron interactions needs to be investigated theoretically.

In short, two-photon physics is an interesting and viable addition to the STAR physics program.

We would like to thank our STAR colleagues for their support for and comments about this work.

References

[1] Baron, N. and Baur, G., Phys. Rev. **C49**, 1127 (1994).

[2] Baur, G. and Ferreira Filho, F., Nucl. Phys. **A518**, 786 (1990).

[3] Berger, C., and Wagner, W., Phys. Rep. 146, **2** (1987).

[4] Berger, C. *et al.*, Z. Phys. **C38**, 521 (1988).

[5] Bringle M.P., "Cosmic Ray Muon Monte Carlo Generator Using the Hemisphere Method", BaBar Note 163, September, 1994; Kral, J. F., "Trigger Rates due to Cosmic Ray Muons," BaBar Note 164, September, 1994.

[6] Brodsky, S., Kinoshita, T., and Terazawa, H., Phys. Rev. **D4**, 1532 (1971).

[7] Budnev, V. M., Ginzburg, I. F., Meledin, G. V., and Serbo V. G., Phys. Rep. **15**, 181 (1975).

[8] Cahn, R. N. and Jackson, J. D., Phys. Rev. **D42**, 3690 (1990).

[9] Chung, S. U., Weygand, D. P., and Willutzki, H. J. "Double-Pomeron and Two-Photon Processes at RHIC," BNL-QGS-02-91 (1991).

[10] *Conceptual Design for the Relativistic Heavy Ion Collider*, BNL 52195, May 1989, Brookhaven National Laboratory.

[11] Evans, L.R., "LEP Status and Future Plans", in *Proc. 1993 Particle Accelerator Conference.*

[12] Greiner, M. Vidović, V. , Hofmann, C., Schäfer, A., and Soff, G., phys. Rev. **C51**, 991 (1995)

[13] Griffiths, D. *Introduction to Elementary Particles* (Wiley, New York, 1987) p.307

[14] Hencken, K., "Photon-Photon Luminosities in Relativistic Heavy Ion Collisions at LHC Energies", NUCL-TH-9503004, May 1995.

[15] Jackson, J. D., *Classical Electrodynamics*, 2nd ed. (Wiley, New York, 1975) p. 722.

[16] Emel'yanov V., Khodinov, A., and Strikhanov, M., "Charm production in peripheral heavy ion collisions." MEPhI-026-95 (1995).

[17] Klein, S., in *Photon '95*, from the Tenth International Workshop on Gamma-Gamma Collisions, Sheffield, England, April 8-13, 1995.

[18] Linkai, D. and Stenlund, E., Comput. Phys. Commun. **59**, 313 (1990).

[19] Morgan D, Pennington, M. R. and Whalley M.R., J. Phys. **G20**, A1 (1994).

[20] Papageorgiu, E., "Coherent Particle Production in Peripheral Nucleus-Nucleus Collisions at Ultra-Relativistic Energies", PhD. Thesis, Munich 1989.

[21] Particle Data Group, Phys. Rev. **D50**, 1173 (1994).

[22] Pumplin, J., Phys. Rev. **D52**, 1477 (1995).

[23] Sjostrand, T., Computer Phys. Commun. **39**, 347 (1986).

[24] Soff, G., Rau, J., Grabiak, M., Muller, B., and Greiner, W., in *The Nuclear Equation of State, Part B.* Eds: Greiner, W., and Stocker, H. (Plenum Press, New York, 1989), p. 579.

[25] STAR Collaboration *Conceptual Design Report of the Solenoidal Tracker At RHIC*, LBL-PUB-5347, 1992.

[26] Wang X.N., personal communication.

[27] Welch, K, "Residual Gas Levels", presented at the *Workshop on Machine Backgrounds at RHIC*, July 19-20, 1995. Copies of the transparencies are available.

[28] Werner, K., Phys. Rep. **232**, 88 (1993).